Accepted at 2024 International Conference on Image Processing (ICIP), Abu Dhabi, UAE, 27-30 October 2024.

FOURIER PTYCHOGRAPHY MICROSCOPY WITH INTEGRATED POSITIONAL MISALIGNMENT CORRECTION

Juliana do Nascimento Damurie da Silva[⋆] *Patrick Horain*

SAMOVAR, Télécom SudParis, Institut Polytechnique de Paris, 91120 Palaiseau, France

ABSTRACT

Fourier Ptychography Microscopy enables reconstructing both intensity and phase high-resolution wide-field images from multiple captures under varying illumination directions. The capture process is classically modeled using a neural network. The reconstructed object is iteratively optimized by gradient descent so the network output matches the captures. Although, this process hinges on a precise estimation of the system geometry. While previous works alternate object image refinement and LEDs positional misalignment correction, we show that geometry estimation can be efficiently integrated into the object reconstruction process, so achieving system self-calibration, and enhancing the quality of reconstructed images.

Index Terms— Fourier Pytchography Microscopy, Position misalignment, Neural Networks

1. INTRODUCTION

Fourier Ptychography Microscopy (FPM) is a technique designed to overcome the space-bandwidth product limitation in microscopy. FPM was first introduced in 2013 [1] as a means of capturing high-resolution and wide-field images with both intensity and phase information from multiple low-resolution images taken under various illumination directions [2]. FPM phase image reconstruction relies on the well-established Gerchberg-Saxton algorithm [3].

In 2018, Jiang et al. [4] proposed to implement the forward process of capturing images from an object as a convolutional neural network. Object reconstruction then consists of minimizing the error between the network output and the actual captures. This allows harnessing the computational power of modern CNN platforms for FPM. Building upon this work, Sun et al. [5] introduced a neural network to combine complex object reconstruction and pupil reconstruction using TensorFlow [6], thereby integrating pupil reconstruction into Jiang's approach.

Zhang et al. [7] in 2021 also use neural networks to correct the pupil optical distortions and complex object reconstruction using total variation regularization. In contrast to the work by Sun et al. [5], Zhang et al. corrected pupil distortions using a neural network approach that combined Zernike polynomials.

Low-cost FPM systems can be implemented using standard microscopes [1]. However, precise positioning of the LEDs and precise distance between the LED array and the sample object are often not available. LEDs misalignment affects the estimation of the illumination angle, which degrades the FPM reconstruction result [2, 8, 9, 10].

Eckert et al. [8] proposed a method for estimating LED positions, but their method is mostly limited to bright field images (e.g. with a limited illumination angle). Some authors alternate steps for image reconstruction and misalignment correction, using simulated annealing [10, 11] or particle swarm optimization [12, 13]. Although, these algorithms depends on an accurate initialization of hyper-parameters as well as a limited search space.

Zhang et al. [14] corrected position misalignment by alternating two neural network models, namely one for correcting misalignments, and the other for reconstructing images and recovering the pupil.

In 2022, Yang et al. [15] proposed a method that uses a neural network to perform simultaneous image reconstruction, misalignment correction, pupil aberration correction, and focus and intensity correction. However, their neural network for correcting the positioning of the LEDs was computationally expensive, and they came to perform alignment outside the neural network by analyzing four of bright field images.

In this work, we propose an FPM implementation that integrates image reconstruction, pupil distortion estimation and correction, and self-calibration of the microscopy's physical parameters in a single neural network at a low computational cost.

2. METHODS

2.1. The principle of FPM

The FPM works by capturing n low-resolution images, where n is the number of LEDs, and reconstructing a complex image of the wavefront, in intensity and phase [2]. Mathematically, the FPM coherent imaging process is described by formula:

⋆ Now with LIRIS, INSA Lyon, 69100 Villeurbanne, France

$$I_n(x,y) = \left| \mathcal{F}^{-1} \left[\mathcal{F} \left(O(x,y) \cdot e^{i(k_{n,x}x + k_{n,y}y)} \right) \cdot \hat{P}(k_x, k_y) \right] \right| \quad (1)$$

where $I_n(x,y)$ represents the low resolution image captured with the n^{th} LED in the spatial domain, $O(x,y)$ is the complex image of the sample object in the spatial domain, $\hat{P}(k_x, k_y)$ represents the pupil function in the frequency domain. A low resolution image I_n is originated from a complex object with intensity and phase, shifted in the frequency plane by $k_{n,x}$ and $k_{n,y}$ (shift due to the LED illumination angle) multiplied with the $\hat{P}(k_x, k_y)$ which represents the limitations of the pupil in the frequency domain.

We describe the pupil and aberrations of an optical system using the Coherent Transfer Function (CTF) [2] $CTF(k_x, k_y)$ and the Zernike polynomial. The model is given by:

$$\hat{P}(k_x, k_y) = CTF(k_x, k_y) \cdot e^{i \sum_{n=0}^{N} a_n Z_n(k_x, k_y)} \quad (2)$$

where the phase term, $\sum_{n=0}^{N} a_n Z_n(k_x, k_y)$ is the optical aberrations in the pupil expressed as a sum of Zernike polynomials $Z_n(k_x, k_y)$ with weights a_n. This model can be used to design and optimize optical systems that compensate for aberrations, leading to improved image quality.

2.2. Neural Network Model

In 2018, Jiang et al. [4] proposed a convolutional neural network that models the Fourier ptychographic forward imaging process. Following the Fineup approach [16], they update the complex object $O(x,y)$ to minimize the difference between the Fourier Transform of the network output and the Fourier Transform of the low-resolution image captured for LED n. This way of calculating the error is widely used [4, 14, 17, 18].

In our approach, we use the same method to jointly reconstruct the complex object $O(x,y)$, recover the pupil aberration, and correct global misalignment. The weights of the neural network are the two real and imaginary planes of the complex object, ten Zernike polynomial weights, and the LED position correction parameters.

2.3. Global LEDs position misalignment correction

The illumination direction for each LED is defined by the position x_0 and y_0 of the center of the LED array, the rotation θ of the LED array, the position (x_n, y_n) of each LED in the array, and the distance h between the LED array and the sample object on the slice. Approximating the light emitted by each LED as a plane wave, their wave vectors in the object plane are directed by:

$$\begin{aligned} k_{n,x} &= -k_0 \frac{x_0 - x_n}{\sqrt{(x_0 - x_n)^2 + (y_0 - y_n)^2 + h^2}} \\ k_{n,y} &= -k_0 \frac{y_0 - y_n}{\sqrt{(x_0 - x_n)^2 + (y_0 - y_n)^2 + h^2}} \end{aligned} \quad (3)$$

where $k_0 = \frac{2\pi}{\lambda}$ and λ is the light wavelength. While these positions may be hard to measure precisely, a number of authors [2, 4, 9, 10] have demonstrated the negative impact of approximate parameters on reconstructed images.

We include the LEDs positioning parameters into the parameters optimized by the network. LED coordinates are updated to positions (x'_n, y'_n):

$$\begin{aligned} x'_n &= x_n \cdot \cos\theta + y_n \cdot \sin\theta \cdot d_x + \Delta x \\ y'_n &= -x_n \cdot \sin\theta + y_n \cdot \cos\theta \cdot d_y + \Delta y \\ h' &= h + \Delta h \end{aligned} \quad (4)$$

where d_x and d_y are the scale factors that adjust the distance between the LEDs on the matrix, and Δx and Δy are the matrix global shifts. Updated positions are then used in Equation 5 to compute the wave vectors.

$$\begin{aligned} k'_{n,x} &= -k_0 \frac{x_0 - x'_n}{\sqrt{(x_0 - x'_n)^2 + (y_0 - y'_n)^2 + (h + \Delta h)^2}} \\ k'_{n,y} &= -k_0 \frac{y_0 - y'_n}{\sqrt{(x_0 - x'_n)^2 + (y_0 - y'_n)^2 + (h + \Delta h)^2}} \end{aligned} \quad (5)$$

Figure 1 shows the architecture of our neural network, with two inputs: the positions $k_{n,x}$ and $k_{n,y}$ of LED n and the corresponding low-resolution captures.

To update the LEDs positions by gradient descent, the resulting pupil disk in the discrete Fourier domain should be differentiable with respect to the LEDs positions, with a non-zero gradient near the disk edges. Spatial Transformer Networks (STN) [19] implement a network layer for image affine transformations with sub-differential bilinear interpolation. Unfortunately, the unneeded generality of affine transformations makes STN computationally expensive. Instead, we developed a custom layer that analytically computes the Zernike polynomials [20] in the translated pupil. The discontinuity at the pupil disk edge is alleviated using a sub-differentiable cone frustum that is easily implemented using a radial Rectified Linear Unit (ReLU) function with saturation.

In the multiplication layer, we multiply the complex object with the pupil after optimizing the positioning parameters. Note that large updates to LED positions will move the object support in the Fourier plane, possibly leaving frequencies out of the support that will no longer be optimized or zeroed. To avoid this, we periodically reset the object to zero and restart object reconstruction with the updated LED positions.

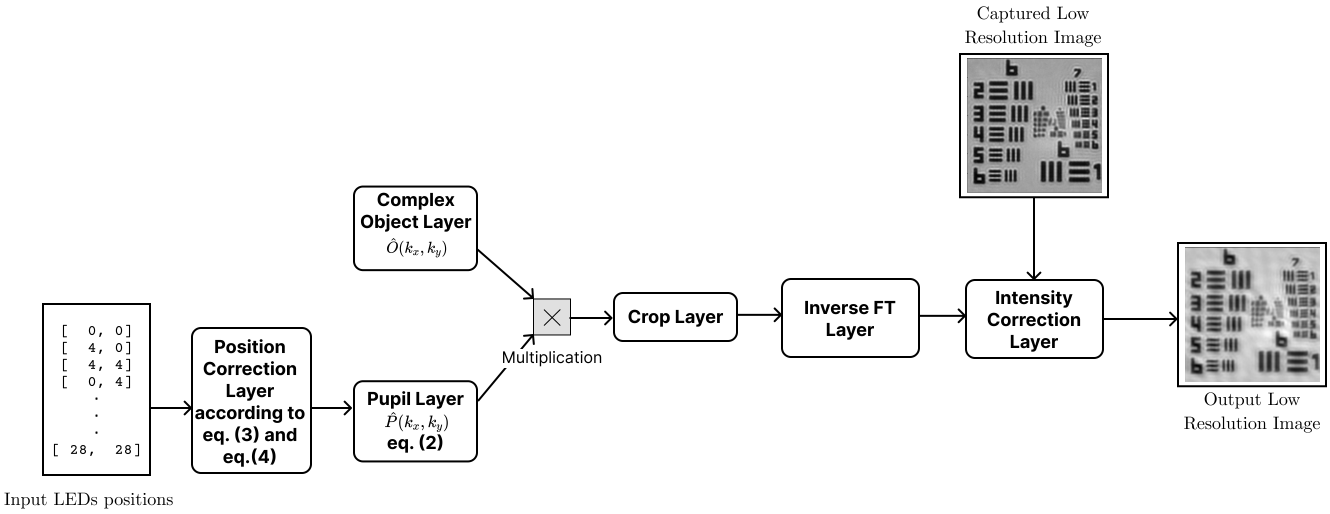

Fig. 1. Architecture of the neural network is derived from [4] to model the image capture process. The input is the current estimation of the LEDs positions. For each LED n, these positions are converted to wave vectors (k_x, k_y) in the Fourier space calculations using equations 3 and 4. The pupil layer is a linear combination of Zernike polynomials that account for optical distortions. The pupil is multiplied by the complex object. Then, the complex object is truncated to match the bandwidth of the low-resolution image. After an inverse Fourier transform, and the LED intensity is corrected using the original low-resolution image. Ultimately, the error between the low-resolution image and the output image generated by the neural network is computed and minimized.

In the crop layer we return the complex object to its original bandwidth, and then perform the inverse Fourier transform. The average intensity is adjusted to match the average of low-resolution image is then corrected to match the average of the corresponding capture, and the output image is compared with the corresponding capture. The objective of minimizing the error function involves reducing the disparity between low-resolution output images produced by the neural network and the low-resolution images captured by the microscope. This discrepancy can be calculated either in the spatial or in the Fourier domain and with either L1 or L2 norms. According to Parseval's equality, the L2 norm yields identical distances in both domains. Re-using code available from [21], we found experimentally that the L1 norm in the Fourier domain resulted in a deeper discrepancy minimum

3. EXPERIMENTS AND RESULTS

We experimented with this approach using captures made by Zheng et al. [1] on the images from 1951 USAF resolution test chart (Table 1).

We compared reconstructions achieved by various FPM implementations. In Fig. 2, we processed Zheng et al.'s captures on a USAF resolution chart [1] using an FPM system that they carefully calibrated by hand, ensuring precise LED positions. Their reconstruction (Fig. 2b) and our neural network

Properties	**Data**
Incident wavelength	0.63 μm
Numerical Aperture of the objective	0.1
Magnification of the objective	2
Pixel Size	2.69 μm
Height	90.88 mm
LEDs array Size	15x15
Distance between LEDs	4 mm

Table 1. Parameters of the captures made by Zheng et al.[1]

without position calibration (Fig. 2c) use exactly the same system position parameters. They achieve similar results in intensity, but the reconstruction by the neural network appears to be better resolved in phase. The position corrections output by our proposed self-calibration (Fig. 2e) are small, and the reconstructed intensity images are close to the previous results, while the phase image is further refined (Fig. 2d).

We also tested the self-calibration robustness to large positioning error, by initializing the LED positions parameters faraway from their actual values: $\Delta x = \Delta y = 4\,\text{mm}$, $\theta = 10^\circ$ and $d_x = d_y = 0.8$. Obviously, this drastically degrades reconstruction results without self-calibration (Fig. 3b). Although, self-calibration can still correctly reconstruct the object both in intensity and phase (Fig. 3c) while optimizing the LEDs positions (Fig. 3d).

Note that, during the LEDs position adjustment, in or-

[1] https://github.com/SmartImagingLabUConn/Fourier-Ptychography

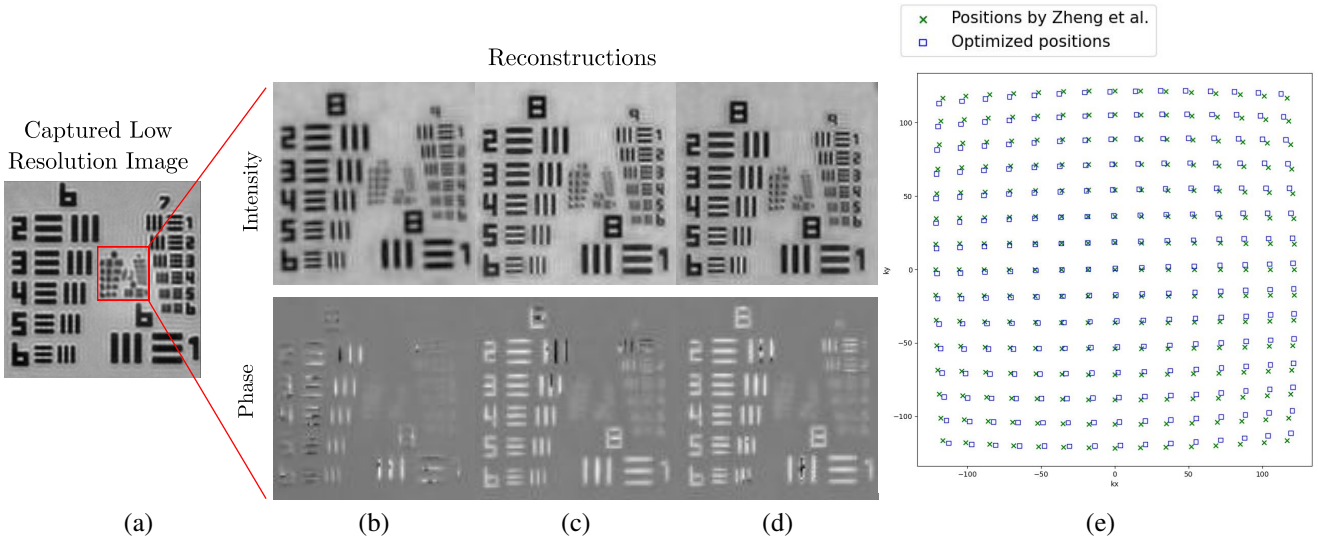

Fig. 2. Comparison of FPM reconstructions on Zheng et al.'s captures of the USAF resolution chart is shown in the central part of the figure where we zoomed in. This comparison highlights the differences in resolution and phase detail achieved by our method versus traditional methods.
(a) Central LED low resolution captured image.
(b) Reconstruction using Zheng et al. Matlab software [1].
(c) Reconstruction by the network architecture without positioning correction.
(d) Reconstruction by the network architecture with the proposed self-calibration of the system geometry.
(e) The calibrated (optimized) wave vectors (k_x, k_y) for the matrix of LEDs.

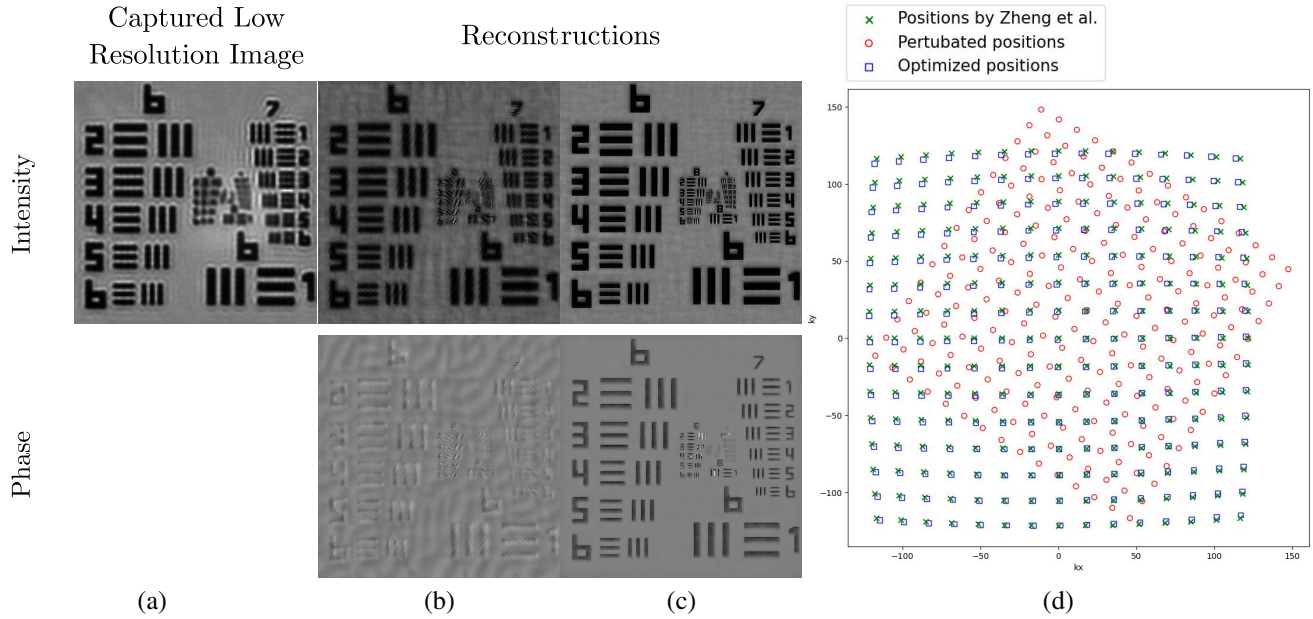

Fig. 3. FPM reconstruction with simulated large positioning error.
(a) Central LED low resolution image captured in intensity (left), reconstruction without positioning correction (2nd column) and reconstruction with the proposed self-calibration of the system geometry (3rd column).
(b) Wave vectors (k_x, k_y) for the matrix of LEDs.

der to avoid leaving high frequencies that would not be adjusted anymore outside the updated object spectral support, we chose to reset the complex object periodically and fully restart the reconstruction from the updated LEDs positions, resulting in a further enhancement (Fig. 4).

This demonstrates the robustness of self-calibration when the LED parameters are very poorly initialized, and drastically alleviates the need for a tedious precise LED position calibration by hand.

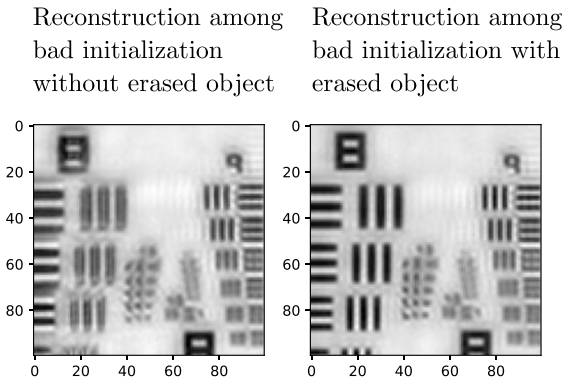

Fig. 4. Periodically resetting the object (right image) allows better reconstruction than without resetting (left).

Properties	**Data**
Incident wavelength	0.532 μm
Numerical Aperture of the objective	0.1
Magnification of the objective	2
Pixel Size	3.45 μm
Height	58 mm
LEDs array Size	8x8
Distance between LEDs	3 mm

Table 2. Bresser[2] microscope capture parameters.

Additionally, we conducted experiments with images we captured using a Bresser Microscope Biolux [2] adapted for FPM with an LED matrix and an Arduino Uno. The parameters of the FPM system are listed in Table 2.

We used a sample of a slice of a mouse brain and initialized the neural network model with an approximate estimation of the LED matrix. The results can be seen in Fig. 5. The first row shows the results of the experiment without self-calibration. In the second row, with auto-calibration, we can see that the spectral support has been rotated, reflecting a rotation in the physical LED matrix. In terms of intensity, the reconstructions are similar, but in terms of phase, we observe a greater aggregation of information. This is evident in the lower part of the phase figure with optimization, where there is more detail compared to the upper figure.

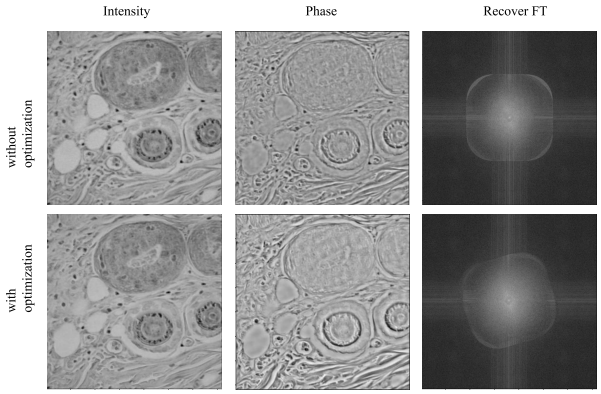

Fig. 5. Reconstruction of a slice of mouse brain . We compare the reconstruction with and without position correction. In the first column we have the reconstructed image in intensity, in the second column the reconstructed image in phase and in the third column the Fourier transform of the reconstructed image. This slice is a courtesy of Dr. Jérôme Polentes.

In our tests, we used 200 epochs to reconstruct a high-resolution image with a size of 564 x 564 pixels. Following Jiang et al. [4], we used the Adam optimizer for the object and pupil optimization layers. After some trials, we selected the Adamax optimizer for the positioning correction layers, utilizing TensorFlow's [6] multi-optimizer feature. On a Tesla T4 GPU, each epoch was executed in 2 seconds.

4. DISCUSSION AND CONCLUSION

We have integrated in the framework of a single neural network: image reconstruction by FPM, pupil distortion estimation and correction, and self-calibration of the microscopy's physical parameters. The method can achieve a close estimation of the system parameters, which allows significantly improving object reconstruction. Unlike other methods, we are able to make corrections of up to one step between the LEDs, as well as being capable of correcting global errors in angles between -10 and +10 degrees. This contrasts with other authors, whose corrections are limited to small errors. As a further improvement, we could make a position correction for each LED and thus perform a more refined correction.

5. ACKNOWLEDGMENTS

This work was supported by *CARNOT Télécom et Société Numérique*.

[2] https://www.bresser.de/fr/emeline/BRESSER-Microscope-Biolux-NV-20x-1280x-avec-Camera-HD-USB.html

6. REFERENCES

[1] G. Zheng, R. Horstmeyer, and C. Yang, "Wide field, high-resolution fourier ptychographic microscopy," *Nature Photonics*, vol. 7, no. 9, pp. 739–745, 2013.

[2] G. Zheng, *Fourier ptychographic imaging: a MATLAB tutorial*. San Rafael, CA: Morgan & Claypool Publishers, 2016.

[3] R. W. Gerchberg and W. O. Saxton, "A practical algorithm for the determination of phase from image and diffraction plane pictures," *Optik*, vol. 35, no. 2, pp. 237–246, 1972.

[4] S. Jiang, K. Guo, J. Liao, and G. Zheng, "Solving fourier ptychographic imaging problems via neural network modeling and tensorflow," *Biomedical Optics Express*, vol. 9, no. 7, pp. 3306–3319, 2018.

[5] M. Sun, X. Chen, Y. Zhu, D. Li, Q. Mu, and L. Xuan, "Neural network model combined with pupil recovery for fourier ptychographic microscopy," *Optics Express*, vol. 27, no. 17, pp. 24 161–24 174, 2019.

[6] M. Abadi, A. Agarwal, P. Barham, E. Brevdo, Z. Chen, C. Citro, G. S. Corrado, A. Davis, J. Dean, M. Devin, S. Ghemawat, I. Goodfellow, A. Harp, G. Irving, M. Isard, Y. Jia, R. Jozefowicz, L. Kaiser, M. Kudlur, J. Levenberg, D. Mané, R. Monga, S. Moore, D. Murray, C. Olah, M. Schuster, J. Shlens, B. Steiner, I. Sutskever, K. Talwar, P. Tucker, V. Vanhoucke, V. Vasudevan, F. Viégas, O. Vinyals, P. Warden, M. Wattenberg, M. Wicke, Y. Yu, and X. Zheng, "TensorFlow: Large-scale machine learning on heterogeneous systems," 2015, software available from tensorflow.org. [Online]. Available: https://www.tensorflow.org/

[7] Y. Zhang, Y. Liu, S. Jiang, K. Dixit, P. Song, X. Zhang, X. Ji, and X. Li, "Neural network model assisted fourier ptychography with zernike aberration recovery and total variation constraint," *Journal of Biomedical Optics*, vol. 26, no. 3, p. 036502, 2021.

[8] R. Eckert, Z. F. Phillips, and L. Waller, "Efficient illumination angle self-calibration in fourier ptychography," *Applied Optics*, vol. 57, no. 19, pp. 5434–5442, 2018.

[9] L.-H. Yeh, J. Dong, J. Zhong, L. Tian, M. Chen, G. Tang, M. Soltanolkotabi, and L. Waller, "Experimental robustness of fourier ptychography phase retrieval algorithms," *Optics Express*, vol. 23, no. 26, pp. 33 214–33 240, 2015.

[10] J. Sun, Q. Chen, Y. Zhang, and C. Zuo, "Efficient positional misalignment correction method for fourier ptychographic microscopy," *Biomedical Optics Express*, vol. 7, no. 4, pp. 1336–1350, 2016.

[11] A. Pan, Y. Zhang, T. Zhao, Z. Wang, D. Dan, M. Lei, and B. Yao, "System calibration method for fourier ptychographic microscopy," *Journal of Biomedical Optics*, vol. 22, no. 9, pp. 1–11, 2017.

[12] Y. Zhu, M. Sun, P. Wu, Q. Mu, L. Xuan, D. Li, and B. Wang, "Space-based correction method for led array misalignment in fourier ptychographic microscopy," *Optics Communications*, vol. 514, 2022.

[13] Y. Chen, T. Xu, J. Zhang, J. Zhang, and J. Li, "Precise and independent position correction strategy for fourier ptychographic microscopy," *Optik*, vol. 265, 2022.

[14] J. Zhang, X. Tao, L. Yang, R. Wu, P. Sun, C. Wang, and Z. Zheng, "Forward imaging neural network with correction of positional misalignment for fourier ptychographic microscopy," *Optics Express*, vol. 28, no. 16, pp. 23 164–23 175, 2020.

[15] D. Yang, S. Zhang, C. Zheng, G. Zhou, L. Cao, Y. Hu, and Q. Hao, "Fourier ptychography multi-parameter neural network with composite physical priori optimization," *Biomedical Optics Express*, vol. 13, no. 5, pp. 2739–2753, 2022.

[16] J. R. Fienup, "Phase retrieval algorithms: a comparison," *Applied Optics*, vol. 21, pp. 2758–2769, 1982.

[17] A. M. Maiden and J. M. Rodenburg, "An improved ptychographical phase retrieval algorithm for diffractive imaging," *Ultramicroscopy*, vol. 109, no. 10, pp. 1256–1262, 2009.

[18] J. R. Fienup and C. C. Wackerman, "Phase-retrieval stagnation problems and solutions," *J. Opt. Soc. Am. A*, vol. 3, no. 11, pp. 1897–1907, 1986.

[19] M. Jaderberg, K. Simonyan, and A. Zisserman, "Spatial transformer networks," *Advances in Neural Information Processing Systems*, vol. 28, 2015.

[20] E. Bostan, R. Heckel, M. Chen, M. Kellman, and L. Waller, "Deep phase decoder: self-calibrating phase microscopy with an untrained deep neural network," *Optica*, vol. 7, pp. 559–562, 2020.

[21] D. Fuoli, L. Van Gool, and R. Timofte, "Fourier space losses for efficient perceptual image superresolution," in *Proceedings of the IEEE/CVF International Conference on Computer Vision*, 2021, pp. 2360–2369.